## CHAPTER 3

## PREPARATION, CHARACTERIZATION AND ANALYTICAL TECHNIQUES

### 3.1 Introduction

The search for hydrogenated amorphous silicon (a-Si:H) with improved properties (low defect density, higher carrier mobility, and enhanced stability, etc.) has led researchers to explore a large number of deposition methods and, within each of them, the effects of each process parameter. Amorphous silicon films produced by the dissociation of hydride gases have low defect density which allows doping compared to films produced by evaporation of a silicon target or by sputtering in the absence of hydrogen. Silane ($SiH_4$) is the most common source gas in a-Si:H deposition even though other hydrides ($Si_2H_6$, $Si_3H_8$, $SiF_4$, $Si_2F_6$, $SiCl_4$, $SiH_2Cl_2$, $SiH_3F$ and $SiH_2F_2$) source gases have been used [1].

Radio frequency (rf) Plasma Enhanced Chemical Vapour Deposition (PECVD) of 13.56 MHz frequency is the most widely used deposition technique because it combines low temperature operation and the possibility of scaling-up the size of the substrates. Nevertheless, for this project, a direct current (d.c.) PECVD system is being used to deposit a-Si:H films because it is more economical to set up, easier and more flexible to operate.

The a-Si:H films studied in this work were deposited on c-Si and glass substrates. The films deposited on glass substrates were used for the optical transmission spectroscopy and dark-conductivity measurements while the films on c-Si substrates were used for infrared spectroscopy. For the XRD measurements and AFM imaging, films deposited on both c-Si and glass substrates were used.

The thin film deposition system and preparation procedures were presented in section 3.2 and 3.3 respectively. The optical spectroscopy technique and calculation

techniques of various parameters obtained from the spectrum were detailed in section 3.4. Section 3.5 presented the measurement technique using the FTIR spectrometer and determination of the integrated intensity under absorption peak. The XRD technique and analytical technique of the spectrogram were presented in section 3.6 while section 3.7 discusses the AFM imaging technique. This chapter ends with the explanation of dark-conductivity measurement technique.

## 3.2 Direct Current (d.c.) Plasma Enhanced Chemical Vapour Deposition (PECVD) System

The films studied in this work were deposited on c-Si and glass substrates using our in-house horizontal d.c. plasma enhanced chemical vapour deposition (PECVD) system. This system, which was designed and built in the Solid State Research Laboratory, University of Malaya have been producing considerable quality amorphous silicon thin films samples by earlier researchers [2,3]. However minor modifications were done on this system for this work in order to produce improved quality thin films with desired parameters.

A schematic diagram of the system is presented in figure 3.1. The system consists of various sub-systems, that is the reaction chamber, the pumping system, the gas distribution system, the detoxification system and the electrical circuitry. All these sub-systems will be described in more detail below.

### 3.2.1 The Reaction Chamber

The d.c. horizontal plasma glow discharge reaction chamber, which is a cylindrical stainless steel vessel, was first designed by K.S. Wong [4]. The detailed arrangement of the reaction chamber and its dimensions is shown in figure 3.2. The cylindrical stainless steel is covered horizontally by two stainless steel plates (front and back plates). Both ends of the reaction chamber have a ring groove which fits in the

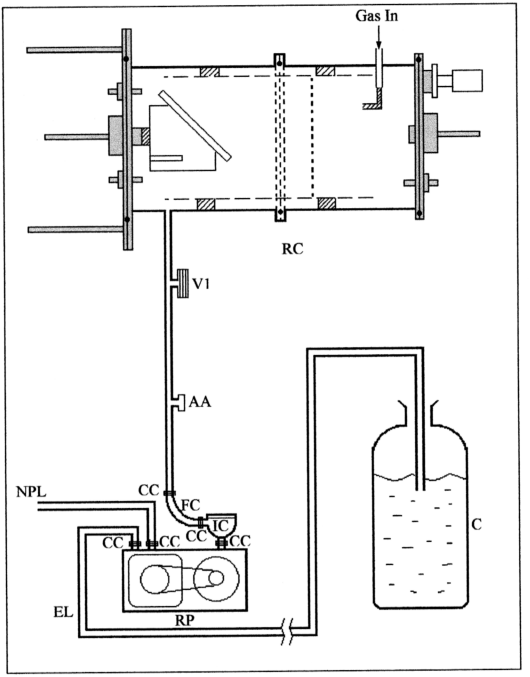


Legend:

AA = Air Admittance Valve
C = Container (containing $KMnO_4$ solution)
CC = Edwards clipped couplings
EL = Exhaust line
IC = Inlet catch-pot
FC = Edwards flexible coupling
NPL = Nitrogen purging line
RC = Reaction chamber
RP = Edwards rotary pump
V1 = Edwards Speedivalve (Roughing valve)

Figure 3.1: The d.c. Plasma Enhanced Chemical Vapour Deposition (PECVD) system illustrating the various sub-systems

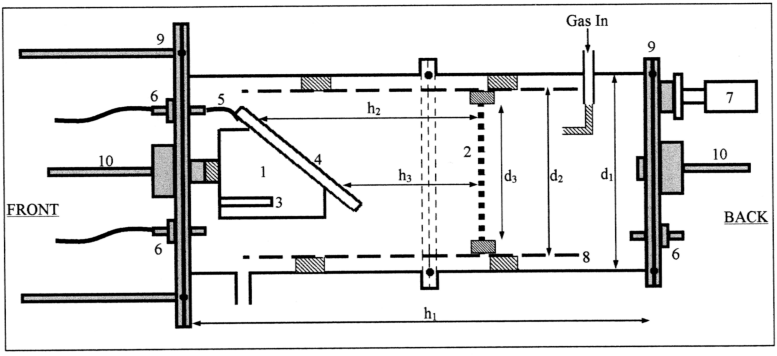


Legend:

| | | |
|---|---|---|
| 1) Aluminium block<br>2) Anode (Stainless steel mesh wire)<br>3) Cartridge heater<br>4) Cathode (Sample holder)<br>5) Chromel-alumel thermocouple | 6) Electrical leadthroughs<br>7) Pirani vacuum gauge head<br>8) Quartz cylinder tube<br>9) Stainless steel cover plates<br>10) Stainless steel rotary shafts | $d_1$ = 14.2 cm; Reaction chamber diameter<br>$d_2$ = 10.0 cm; Quartz tube diameter<br>$d_3$ = 8.2 cm; Mesh wire (anode) diameter<br>$h_1$ = 30.0 cm; Reaction chamber width<br>$h_2$ = 9.7 cm; distance between electrodes (upper part)<br>$h_3$ = 5.0 cm; distance between electrodes (lower part) |

Teflon  Viton O-ring

Figure 3.2: A Schematic diagram of the reaction chamber highlighting various components and dimensions

Viton O-ring tightly. This is to make sure that the chamber maintains a high vacuum during deposition. The lowest pressure achieved prior to gas entry is about $2 \times 10^{-2}$ mbar when the system is fully pumped down using an E2M 28 Edwards rotary pump. The front plate carries a teflon rod (2 cm in diameter) at the centre which supports the aluminium block (used as a sample holder). It also supports two lead-throughs for electrical connections to the power supply and temperature controller and thermocouple connections. The back plate holds a gauge-head, which connects the chamber to the Pirani PR10-S pressure meter and an electrical lead-through for the anode.

The aluminium block was designed so that it is fixed slanted at 45°. The upper and lower part of the cathode is separated 9.7 cm and 5.0 cm from the anode respectively. For characterization purpose the sample position is fixed since the distance between anode and cathode is an important deposition parameter that can affect the thin film properties.

The minor modifications done to the sample holder is as illustrated in figure 3.3. In the previous design, the thermocouple is fixed onto the sample holder. In this work, the substrate holder is drilled so that the thermocouple wire can be inserted through it and be attached directly onto the substrate. This is to ensure that the temperature recorded is the temperature of the sample and not of the sample holder.

### 3.2.2 The Pumping System

The vacuum pump that has been used in this lab is Edwards E2M 28 rotary pump. The system is evacuated and maintained at the desired pressure during all depositions. The pressure is detected by a special corrosion resistant gauge-head (PR10-S) and monitored by a control unit (Edwards Pirani 11). An inlet catch-pot is attached to this pump to ensure that any vapour can be absorbed effectively. This catch-pot is

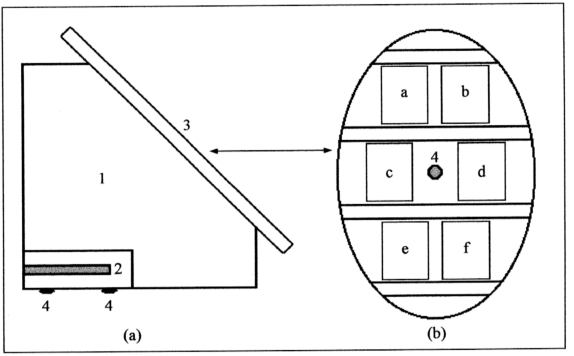


Legend:

1) Aluminium block
2) Cartridge heater
3) Sample holder
4) Screws
a, b, c, d, e, f are positions of the samples

Figure 3.3: A schematic diagram of sample holder (a) side view, (b) front view illustrating the position of sample.

connected directly to the reaction chamber via Edwards flexible coupling as illustrated previously in figure 3.1.

This system equipped with a security tools, that is the 3 kVA Uninterruptible Power Supply (UPS). This equipment is very important as it can sustain the power supply for about 40 minutes when there is any power interruption. This can make sure that the silane gas, which is hazardous, can be handled efficiently during deposition. The rotary pump is equipped with a purging line, which bleeds in nitrogen gas. This is to dilute the excess silane gas, which later on be sent out via exhaust line to the detoxification system outside the lab.

### 3.2.3 The Gas Distribution System

The gases used in this work are silane ($SiH_4$), helium (He), oxygen-free nitrogen (OFN) and nitrogen ($N_2$). All these gases are distributed to the reaction chamber via a gas distribution system, which is schematically shown in figure 3.4. The gas lines are made of 0.25" stainless steel tubing and are connected using Swagelock connectors and valves from the tank (inside gases room) to a gas distribution panel and then to the reaction chamber.

For safety purposes, the silane gas is placed inside a gas cabinet, which has a proper exhaust system to remove silane in case of leakage. The silane has a special gas regulator model Soxal 450-BS4-100 with special purging system. This purging system is connected to a nitrogen gas cylinder (figure 3.4). This special gas regulator has a pneumatic valve, which allows gas through it only when the pressure of OFN is about 50 psi. This OFN gas is connected to the regulator through a safety system. This safety system, which particularly used for silane gas can stop the silane flow to the chamber instantly in the case of emergency.

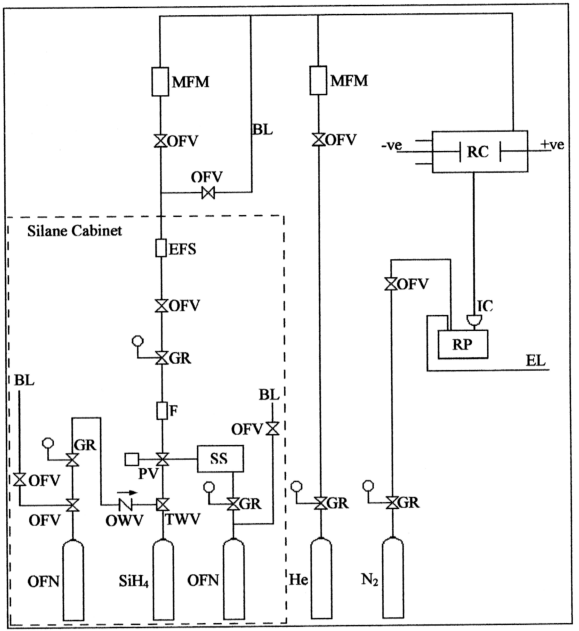


Legend:

| | | |
|---|---|---|
| BL = Bypass Line | IC = Inlet Catchpot | PV = Pneumatic Valve |
| EFS = Excess Flow Switch | MFM = Mass Flowmeter | RC = Reaction Chamber |
| EL = Exhaust Line | OFN = Oxygen-free Nitrogen | RP = Rotary Pump |
| F = Filter | OFV = On-off Valve | SS = Safety System |
| GR = Gas Regulator | OWV = One Way Valve | TWV = Three Way Valve |

Figure 3.4: Schematic diagram for the gas distribution system for the d.c. deposition a-Si:H in this work

From the gas distribution panel, the gases are distributed to different systems in the laboratory using valves. On entering the PECVD system used in this work, each gas passes through a Hastings mass flow controller (model HFC-C202), which is calibrated for each particular gas, to monitor the gas flow-rate. As shown in figure 3.4, a gas line bypassing the mass flow controller to make it possible to pump out the silane gas in case of blockage within the mass flow controller.

### 3.2.4 The Detoxification System

The purpose of this system is to ensure dilution of unreacted toxic gas ($SiH_4$ gas) and chemically change it into a non-toxic form. Normally the nitrogen gas is used to dilute this unreacted $SiH_4$ from the reaction chamber as illustrated in figure 3.4. The exhaust pipe from the rotary pump is immersed into a container, which contains potassium permanganate solution ($KMnO_4$). The chemical reaction involved is,

$$2KMnO_4 + SiH_4 \rightarrow 2KMnO_2 + K_2SiO_4 + 2H_2$$

The solution is changed every time its colour changes.

### 3.2.5 The Electrical Circuitry

The electrical circuitry of the PECVD system consists of two 240V AC power supply, which are connected to the cartridge heater and to the electrodes of the reaction chamber as can be seen in figure 3.5. The temperature controller (Sigma MDC4S) maintains the deposition temperature via a cartridge heater and a chromel-alumel thermocouple. The other 240V AC main supply, which is amplified by a step-up transformer with an input of 240 V and output of 3 kV, is then rectified by a full wave diode rectifier bridge which consists of 32 diodes. The transformer is immersed in a container filled with oil to keep it cool. A series of resistor is used to control the current during preparation and hence protecting the transformer from any current overload.

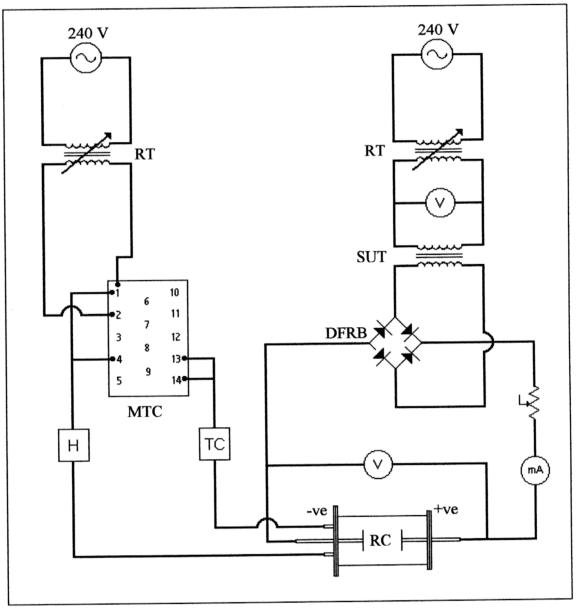


Legend:

DFRB = Diode Full Rectifier Bridge
H = Heater
MTC = Microprocessor Temperature Controller (Sigma MDC4S)
RC = Reaction Chamber
RT = Regulating Transformer
SUT = Step-up Transformer
TC = Chromel-alumel Thermocouple

Figure 3.5: A Schematic diagram of the electrical circuitry of PGD2 illustrating both the high voltage power supply and the heater circuitries.

An Iwatsu high voltage probe (model HV-P30) and an Iwatsu oscilloscope (model SS-5710) are used to monitor the high d.c. potential across the electrodes of the reaction chamber. Since only a low current flow during ionization, an analog milliammeter is used, which has a range of 0 – 100 mA.

### 3.3 Thin Film Deposition Procedures

As discussed in the chapter 2, the silane is a toxic gas that reacts explosively with both air and water vapour. Therefore, it is essential to make sure that the system is absolutely free of any leakage. This also prevents the samples from any impurities that can affect their properties. The post-deposition procedure is also necessary as the pre-deposition procedure because it can ensure that the system is free from excess silane before taking out the samples. Very low concentration of silane left in the lines will form white powder which collects at points in the lines where there are needle valves and flow controllers inlet. This white powder when closely packed can block gas lines and can be dangerous as high pressure built-up at these blocked points can cause severe leakage in the lines.

#### 3.3.1 The Cleaning Procedure

In this work, two types of substrates are used, that is p-type crystal silicon wafer and Corning glass. The crystal silicon wafer has a resistivity of 1-7 $\Omega cm^{-1}$. These substrates have to be thoroughly cleaned by specific techniques, which will be described below prior to deposition as the adhesion of a thin film to the substrate depends critically on the conditions at the substrates surface. Even a monomolecular layer of a contaminant on the surface can change the force of adhesion by orders of magnitude thus reducing the sticking probability of the film to the substrates. This also results in peeling of the film after deposition when removed from the vacuum chamber.

Prior to cleaning, the crystal silicon is cut into small pieces (± 2 cm × 2 cm) and rinsed with deionized water. They are then boiled in a solution of $H_2O$ : $H_2O_2$ : HCl with a ratio of 86 : 11 : 3 for 10 minutes. After that, they are rinsed with deionized water to remove any excess inorganic solution. Then, the substrates are immersed in the solution of $H_2O$ : $H_2O_2$ : $NH_4OH$ with a ratio of 7 : 3 : 3 for 10 minutes to eliminate any organic contamination. It is followed by the rinsing process again. Next, the substrates are dipped in the solution of $H_2O$ : HF (10 : 1) for 10 minutes. Finally, the substrates are rinsed with deionized water several times and dried with a hair dryer.

For Corning glass substrates, the procedure of cleaning is as follows. Initially the substrate is immersed in a beaker of soap water which is immersed into the ultrasonic bath and agitated for about 15 minutes. Then, the substrates are rinsed with distilled water. These substrates are then cleaned in acetone and ethanol for a few minutes to remove oil contaminants. Finally, the substrates are cleaned again with distilled water and dried with a hair dryer.

### 3.3.2 Pre-deposition Procedure

Traces of left over deposits on the walls of the reaction chamber as a result of previous deposition must be removed and cleaned prior to deposition. The vigorous use of wet sandpaper on all the metal surfaces is found to be the most effective technique of removal. Once all parts of the reaction chamber are cleaned, the cleaned substrates are then introduced into the chamber. Viton O-rings are securely placed between plates (front and back) and the deposition chamber. Vacuum grease is applied thinly to the Viton O-ring to ensure a good seal. The Pirani gauge-head, electrodes, heater and the thermocouple are then fixed to their positions as shown in figure 3.2.

Before switching on the pump, all the valves (roughing valve, V1 and air admittance valve, AA) (refer to figure 3.1) are closed. The lines are evacuated until a

pressure of $2 \times 10^{-2}$ mbar is achieved. A higher pressure could be indicative of a leakage and should be fixed before any deposition can takes place. When the required pressure is reached, V1 is opened. At this point, the pressure monitored is the pressure inside the deposition chamber. Then, the gas lines are opened stage by stage from deposition chamber to the gas cylinder. At the same time, the cathode is heated to the desired temperature and is maintained by using Sigma MDC4S microprocessor temperature controller. The system is ready for the deposition when the pressure of the whole system is around $2 \times 10^{-2}$ mbar.

### 3.3.3 Deposition Procedure

The deposition temperature and pressure for all samples studied in this work are maintained at 200°C and 1.5 mbar respectively. Prior to admitting other gases into the deposition chamber, it is necessary to introduce the nitrogen gas into the rotary pump to dilute the unreacted $SiH_4$ gas from the deposition chamber. The line pressure at the oxygen-free nitrogen gas regulator (the right one in figure 3.4) is fixed at 50 psi to operate the gas safety system. This will automatically open the pneumatic valve and allow the $SiH_4$ gas to flow through it. The excess flow switch (EFS) is utilized in this line to stop any uncontrollable excess $SiH_4$ that flow through this line. The EFS will activate if the pressure inside this line is suddenly increase and the alarm in the safety system will ring.

The release of the silane gas into the reaction chamber is followed by the helium (He) gas at the desired flow-rate. The d.c. power supply is then turned and the voltage across the electrodes are fixed to maintain an ionization current at 10 mA. The deposition time is recorded from the time the d.c. power supply is turned on until it is turned off. During the deposition, all parameters such as the deposition pressure, the gas

flow-rate and the ionization current are observed every 10 minutes to ensure that they are maintained at the desired setting.

### 3.3.4 Post-deposition Procedure

To terminate the deposition, the voltage supply across the electrodes is turned off and the helium and silane gas regulators are closed. The gas lines are pumped down until the pre-deposition pressure of $2 \times 10^{-2}$ mbar is achieved. This can also be confirmed by monitoring the flow-meter, which shows a zero flow-rate reading for all gases when lines are fully evacuated. This will confirm that there are no excess gases left in the gas line. Then, the lines are purged with oxygen-free nitrogen (OFN, the left one in figure 3.4) for several cycles for duration of about 10 minutes for each cycle. This technique is detailed and discussed below.

### 3.3.5 Gas Line Purging Technique

Purging of the gas lines is necessary not only just after deposition but should also be done when the system is not used for a long period of time. Purging the lines by just passing a flow of oxygen-free nitrogen (OFN) through the system for a considerable period of time may leave unacceptable levels of air and moisture in the system especially in 'dead-ends' in the gas line. A much more efficient technique is by a cyclic variation in pressure, preferably a pressurization followed by an evacuation. The evacuation and purging operation is repeated several times where the period for each cycle is 10 minutes. The pressure of about 70 psi is found to be the most effective pressure used to purge the gas lines.

### 3.4 Optical Characterization

Considerable theoretical and experimental investigations on the optical behaviour of thin films primarily deal with optical reflection, transmission, and absorption properties, and their relation to the optical constants of films. The Jasco V-570 UV-Vis-NIR Spectrophotometer is used in this work to study the optical properties of the samples deposited on Corning glass substrates. The schematic block diagram of this equipment is shown in figure 3.6. Generally, this spectrophotometer can be divided into two main systems, which are optical system and electrical system [9].

#### 3.4.1 UV-Vis-NIR Optical Spectroscopy Technique

In this work, the optical transmission spectroscopy is performed within the scanning range of 200 to 2500 nm that is from ultra-violet to near infrared region. Deuterium discharge tube (200 to 350 nm) is used as a light source in the ultra-violet region while iodine tungsten lamp is used as a light source for the visible/ near infrared region. Both of these lamps function as a light source. This beam of light then travels through a monochromator and is emitted as a monochromatic light source. Next, a mirror will then split this light beam into two light beams, which is then transmitted through the sample and reference substrate separately. These light beams will then travel to a photomultiplier tube, which acts as a light detector in this system.

The photomultiplier tube converts the light into an electrical signal, which then is decoded into a digital form. A software will then process this signal and produced as output displayed in the form of a spectrum. UV-Vis-NIR used in this work is automated and controlled by a microcomputer.

The scanning measurement begins with the scanning of spectral baseline by placing two glass slides, which are used as substrates for the film in both the reference and sample holders (see figure 3.6). Once the baseline spectrum is obtained, the glass

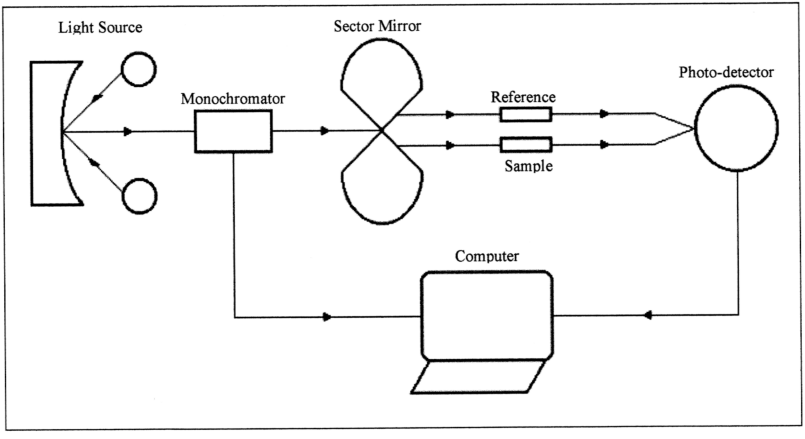


Figure 3.6: A Block Diagram of the Optical Transmission Set-up

slide in the sample holder is removed and is replaced by the a-Si:H thin film sample. The instrument is now ready to execute the transmission spectrum of the a-Si:H sample.

### 3.4.2 Determination of Film Thickness and Refractive Index

Figure 3.7 shows a typical transmission spectrum for a-Si:H thin film sample. The film thickness and its refractive index can be determined using the technique proposed by J.C. Manifacier et. al. [6]. The envelope method, which is particularly used in determining this optical constant, produces the sets of $T_{max}$ and $T_{min}$ values. The basic equation for the interference fringes to occur is

$$2nd = m\lambda \qquad \ldots(4.1)$$

where m denotes the order of the fringes, which has an integer value (for maxima) and a half integer (for minima), n is the refractive index and d is the film thickness.

For a thin film sample, which bounded by two transparent media (see figure 3.8) with refractive indices, $n_0$ and $n_1$, the transmission of the layer is given by

$$T = \frac{16n_0n_1n^2\alpha}{C_1^2 + C_2^2\alpha^2 + 2C_1C_2\alpha\cos\left(\frac{4\pi nt}{\lambda}\right)} \qquad \ldots(4.2)$$

where $C_1 = (n+n_0)(n_1+n)$

$C_2 = (n-n_0)(n_1-n)$

$\alpha = \exp\left(\frac{-4\pi kt}{\lambda}\right) = \exp(-Kt)$

K is the absorption coefficient of the thin film.

The above expression is applicable only in the weak absorption region with

$k^2 << (n - n_0)^2$

and $k^2 << (n - n_1)^2 \qquad \ldots(4.3)$

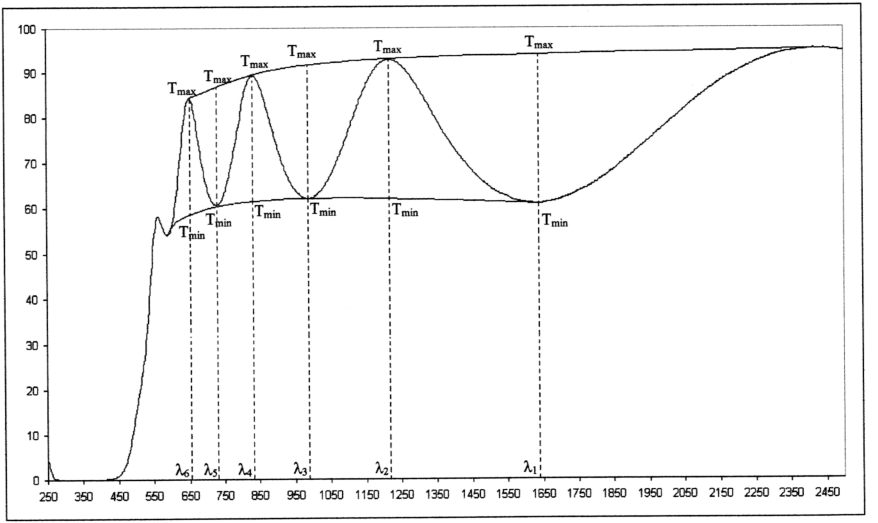


Figure 3.7: A typical spectrum with interference fringes illustrating the envelope method, which is used to calculate the optical constants of the film.

In usual case, where $n >> n_1$, corresponding to a semiconducting film on a transparent non-absorbing substrate, $C_2 < 0$, the extreme values of the transmission are given by the formulae

$$T_{max} = \frac{16 n_0 n_1 n^2 \alpha}{(C_1 + C_2 \alpha)^2} \qquad \ldots(4.4)$$

$$T_{min} = \frac{16 n_0 n_1 n^2 \alpha}{(C_1 - C_2 \alpha)^2} \qquad \ldots(4.5)$$

By combining equations (4.4) and (4.5), Lyashenko and Miloslavskii (1964) developed an iterative method allowing the determination of n and $\alpha$

$$n = \left( N + \sqrt{N^2 - n_0^{\,2} n_1^{\,2}} \right)^{1/2} \qquad \ldots(4.6)$$

where

$$N = \frac{n_0^{\,2} + n_1^{\,2}}{2} + 2 n_0 n_1 \frac{T_{max} - T_{min}}{T_{max} T_{min}} \qquad \ldots(4.7)$$

The thickness, d of the thin film can be calculated from sets of refractive indices and wavelengths derived above

$$d = \frac{M \lambda_1 \lambda_2}{2\left[ n(\lambda_1)\lambda_2 - n(\lambda_2)\lambda_1 \right]} \qquad \ldots(4.8)$$

where M is the number of oscillations between two extremas (M=1 between two consecutive maxima or minima), $\lambda_1$, $n(\lambda_1)$ and $\lambda_1$, $n(\lambda_1)$ are the corresponding wavelengths and indices of refraction at that particular wavelength respectively.

Equation 4.6 depends critically on the transmission intensity of the light and the fitting of the envelope on to the extremas of the interference fringes. This introduces higher probabilities of inaccuracies. To overcome this, the E.A. Davis technique [8] is incorporated into the J.C. Manifacier technique [6]. The basic equation for the interference fringes (equation 4.1) is used on the wavelength positions of the maximas

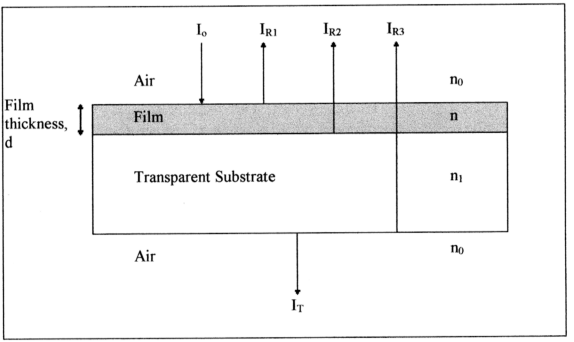


Legend:

$n_0$ = refractive index of air
n = refractive index of film
$n_1$ = refractive index of substrate
$I_o$ = incident light
$I_{R1}$ = reflected light at air-film interface
$I_{R2}$ = reflected light at film-substrate interface
$I_{R3}$ = reflected light at substrate-air interface
$I_T$ = transmitted light

Figure 3.8: A Schematic Structure of a-Si:H Thin Film Sample.

and minimas of the fringes. A plot of $m\lambda/2$, which is equal to nd (refer to equation 4.1) versus $\lambda$, is produced where the m value is initially guessed. The first correct m value will produce a curve where nd decreases monotonically with $\lambda$. Since equation 4.6 is most accurate where the transmission intensity is the highest, the n value calculated by this technique at the maxima or minima in the longest wavelength region in the spectrum is used. Using the correct m value at this point, the film thickness, d is determined. Since d does not vary with wavelength, the n values at the other maximas and minimas are determined by dividing the nd value at each extrema point by this film thickness value.

The refractive indices for the whole spectrum are determined by fitting the n values calculated above into the Cauchy equation [7]

$$n = \frac{a}{\lambda^2} + b \qquad \ldots(4.9)$$

where a and b are constants.

### 3.4.3 Determination of Non-Silicon Atoms Content in the Film

The dispersion curve of the refractive index versus wavelength obtained above is fitted on to the Wemple and DiDomenico equation [9]

$$n^2(\omega) - 1 = \frac{E_d E_o}{E_o^{\,2} - E^2} \qquad \ldots(4.10)$$

by rearranging the equation in the form

$$\frac{1}{n^2(\omega) - 1} = \frac{E_o}{E_d} + \frac{E^2}{E_d E_o} \qquad \ldots(4.11)$$

where n = refractive index of a-Si:H

$E_d$ = dispersion energy

$E_o$ = single oscillation energy

E = photon energy

The $E_d$ and $E_o$ values are determined from the linear section of $1/(n^2-1)$ versus $E^2$ using following equations extracted from equation 4.1

$$E_o = \sqrt{\frac{1}{mc}} \qquad \ldots(4.12)$$

$$Ed = \sqrt{\frac{c}{m}} \qquad \ldots(4.13)$$

where m is the slope and c is the intercept of the graph.

The density of valence electron, $n_v$ of a-Si is determined from a model proposed by C. Ance et. al [10]

$$n_v = 0.0143\frac{Ed^2}{\varepsilon(0)-1}\times 10^{23}\ \text{cm}^{-3} \qquad \ldots(4.14)$$

where $\varepsilon(0) = n^2$. For c-Si, the the value of $E_d$ and $\varepsilon(0)$ is taken as 38.6 eV and 11.66 respectively, so the density of valence electron for c-Si, $n_s$ is $2 \times 10^{23}$ electron/cm$^3$.

The non-Si atom content in the film can be calculated using the relationship [10]

$$C_H(\%) = \frac{1}{3}\frac{n_v}{n_s}\left(4-\sqrt{\frac{E_d}{2.8}}\right)\times 100\% \qquad \ldots(4.15)$$

The non-Si atom content calculated from above equation represents the atomic percentage of non-silicon atoms bonded to silicon atom which includes H atoms and impurity atoms like O or N [11].

### 3.4.4 Determination of Optical Energy Gap of the Film

When a light beam shine onto a material (solid, liquid or gas), the photon at certain wavelength will be transmitted, absorbed or reflected depending on the properties of that material. Figure 3.8 illustrates these phenomena. Brodsky et. al. [12] proposed that when light strike the film, there are three possibilities of reflection, $R_1$, $R_2$ and $R_3$ as shown in figure 3.8. The transmission, T through air-film substrate interface is given by this relation [12]

$$T = \frac{I_T}{I_O} = \frac{(1-R_1)(1-R_2)(1-R_3)e^{-\alpha d}}{(1-R_2R_3)\left\{1-\left[R_1R_2+R_1R_3(1-R_2)^2\right]e^{-2\alpha d}\right\}} \quad \ldots(4.16)$$

where $R_1$, $R_2$ and $R_3$ are the reflectance at the air-film, film-substrate and substrate-air respectively. This approximation includes all the non-coherent multiple reflections. Bahl's relations [13] are used to determine the reflectivities

$$R_1 = \frac{(n-1)^2 + k_o^2}{(n+1)^2 + k_o^2} \quad \ldots(4.17)$$

$$R_2 = \frac{(n-n_1)^2 + k_o^2}{(n+n_1)^2 + k_o^2} \quad \ldots(4.18)$$

$$R_3 = \frac{(n_1-1)^2}{(n_1+1)^2} \quad \ldots(4.19)$$

where n and $n_1$ are refractive indices of thin film and substrate respectively, whereas $k_o$ is extinction coefficient. For transparent material, $k_o = 0$.

Equation (4.17), (4.18) and (4.19) can be simplified by taking

$$A = (1-R_1)(1-R_2)(1-R_3) \quad \ldots(4.20)$$

$$B = (R_2R_3) \quad \ldots(4.21)$$

$$C = R_1R_2 + R_1R_3(1-R_2)^2 \quad \ldots(4.22)$$

So,

$$T = \frac{AX}{(1-B)(1-CX^2)} \quad \ldots(4.22)$$

Equation (4.23) can be written in the quadratic form

$$(TC-TBC)X^2 + AX - (T-TB) = 0 \quad \ldots(4.24)$$

which gives a solution of X

$$X = \frac{-A + \sqrt{A^2 + 4CT^2(1-B)^2}}{2CT(1-B)} \quad \ldots(4.25)$$

So the absorption coefficient, α of the thin film at different wavelength can be evaluated using

$$\alpha = \frac{1}{d}\ln\left(\frac{1}{X}\right) \text{ cm}^{-1} \qquad \ldots(4.26)$$

where d is the film thickness.

The absorption coefficient calculated above is used to determine the optical energy gap, $E_g$ of the thin film a-Si:H. The measurement of $E_g$ in amorphous film is commonly deduced from a Tauc's plot of $\sqrt{\alpha E}$ versus E in the strong absorption region [13,14].

### 3.4.5 Determination of Urbach Energy Value of the Film

The equation, which was proposed by Tauc et. al. [13] in strong absorption region can be expressed as

$$\alpha E = A\left(E - E_g\right)^2 \qquad \ldots(4.27)$$

In the region close to the absorption edge, the absorption coefficient varies exponentially with photon energy as in the equation below

$$\alpha(\omega) = A\exp\left[-\beta\left(E_e - \hbar\omega\right)\right] \qquad \ldots(4.28)$$

where $E_e$ is the Urbach energy, A is a constant and ω is an angular frequency. The β value at 300 K is in the range of 10 – 25 $eV^{-1}$. This value is found to be exactly the same as the inverse width of tail state region calculated by Urbach [15]. The width of Urbach tail ($E_e$ value) in a-Si:H is due to the defect or imperfectness in the structure of the film. So $E_e$ can be used to measure the disorder of the film and is determined by using this equation derived from equation 4.28

$$\alpha(E) = \alpha_o \exp\left(\frac{E - E_1}{E_e}\right) \qquad \ldots(4.29)$$

where $E_1$ and $\alpha_o$ are experimentally determined factors. The $E_e$ value is deduced from the slope of the linear part of the graph ln ($\alpha$) versus E near the absorption edge.

### 3.5 Chemical Bonding Analysis

The Perkin-Elmer model 2000 Fourier Transform Infrared (FTIR) spectrophotometer is utilized in this work to obtain the infrared spectrum of a-Si:H thin film deposited on crystal silicon substrate. For this work, the region of interest in the IR study is in the range of 400 – 4000 $cm^{-1}$. Crystal silicon is used as a substrate because of its symmetry and it also does not absorb any infrared photons [16]. FTIR spectroscopy is very valuable technique since it can provide a variety of information on the chemical bonding, the type and concentration of impurities and defects.

#### 3.5.1 Fourier Transform Infrared Spectroscopy Technique

An infrared spectrum represents a fingerprint of a sample with absorption peaks, which correspond to the frequencies of vibrations between the bonds of the atoms making up the material. The vibrations describe the motions of atoms in terms of changes in bond lengths, bond angles, and dihedral or torsional angles. Because each different material is a unique combination of atoms, no two compounds produce the exact same infrared spectrum. Therefore, infrared spectroscopy can result in a qualitative analysis of every different kind of material. In addition, the size of the peaks in the spectrum is a direct indication of the amount of material present.

The bands in infrared spectra can be related to the stretching of a particular chemical bond or the bending of an angle. Usually the infrared absorption bands are attributable to coupled vibrations, that is, vibrations that involve more than one type of motion taking place at the same frequency.

The description of the infrared absorption band by the most predominant contribution leads to the definition of group frequencies that have been found to correlate experimentally with the presence of a particular chemical bond or group. Group frequencies are frequently used to interpret the infrared spectra of organic and inorganic compounds and to determine the functionality of a particular material.

Figure 3.9 shows a simple spectrometer layout. It contains the IR source (emitted from a glowing black-body source), the interferometer (encode the beam into the interferogram signal), the sample (in the sample compartment), the detector (designed to measure the special interferogram signal) and the computer (digitizes the measured signal where the Fourier transformation takes place and then presents the final infrared spectrum). The specific configuration is presented in figure 3.10.

Because there is a need for a relative scale for the absorption intensity, a background spectrum must also be measured. This is normally a measurement with no sample in the beam. This can be compared to the measurement with the sample in the beam to determine the percent transmittance. This technique results in a spectrum which has all of the instrumental characteristics removed. Thus, all spectral features which are present are strictly due to the sample. A single background measurement can be used for many sample measurements because this spectrum is characteristic of the instrument itself.

### 3.5.2 Determination of Integrated Intensity of an Absorption Peak

The band assignments for the principle IR modes in a-Si:H studied by group of researchers are summarized in table 2.1. The integrated intensity of the Si–H wagging band at 640 $cm^{-1}$ has been shown to be proportional to the hydrogen content of the film whatever the film microstructure is [17]. The absorption band at 2000 $cm^{-1}$ and 2090

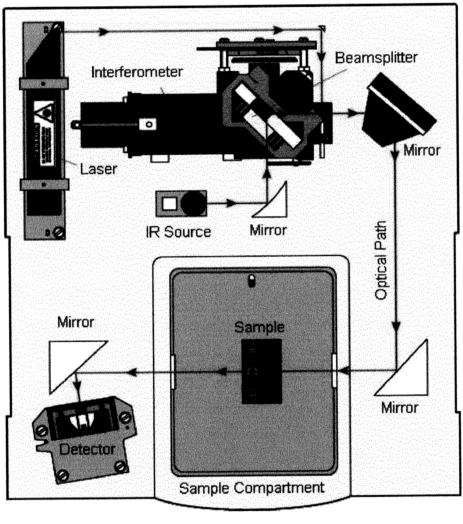


Figure 3.9: A Simple Spectrometer Layout

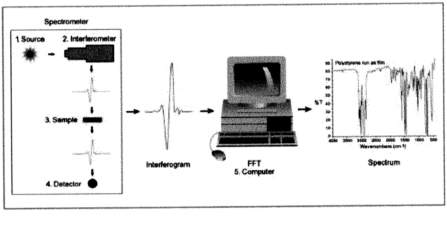


Figure 3.10: The Sample Analysis Process

$cm^{-1}$ corresponds to the Si–H and $SiH_2$ stretching mode respectively. Normally for this work, the bands at 2000 $cm^{-1}$ and 2090 $cm^{-1}$ overlap and form a broad band.

The area under the absorption spectrum can be used to calculate the integrated intensities of the different vibration modes for the a-Si:H. The transmission spectrum from FTIR can be converted into absorption spectrum using this equation

$$\alpha = \frac{1}{d}\ln\left(\frac{100}{T\%}\right) \qquad \ldots(4.30)$$

where d is the film thickness and T% is the transmission percentage. The conversion is shown schematically in figure 3.11. The Gaussian or Doppler lineshape is drawn on to deconvolute component peaks from the absorption spectrum. The general equation for Gaussian lineshape can be expressed in the general form as follows [18,19]

$$\alpha(\omega) = \alpha(\max)\exp\left\{-\frac{\left[4(\ln 2)(\omega-\omega_O)^2\right]}{\Delta\omega}\right\} \qquad \ldots(4.31)$$

where $$\alpha(\max) = \frac{2\sqrt{\ln 2}S_{band}}{\sqrt{\pi}\Delta\omega} \qquad \ldots(4.32)$$

and $$S_{band} = \int \alpha(\omega)\, d\omega \qquad \ldots(4.33)$$

$S_{band}$ is the area under the curve, $\Delta\omega$ is the full width at half maximum (FWHM) of the absorption peak, $\alpha(\max)$ is the maximum absorption coefficient and $\omega_o$ is the peak position. Equation (4.31) can be written in the simpler form

$$y = A\exp[-(Bx)] \qquad \ldots(4.34)$$

where $$A = \frac{\sqrt{B}S_{band}}{\sqrt{\pi}} \qquad \ldots(4.35)$$

$$B = \frac{4\ln(2)}{(\Delta\omega)^2} \qquad \ldots(4.36)$$

$$x = (\omega - \omega_o)^2 \qquad \ldots(4.37)$$

Equation (4.34) is then rewritten as

$$\ln(y) = \ln(A) - B(\omega - \omega_o)^2 \qquad \ldots(4.38)$$

Finally the integrated intensity of the absorption peak representing a bonding configuration can be calculated using

$$I = \int \frac{\alpha(\omega)}{\omega_o} d\omega \qquad \ldots(4.39)$$

or from equation (4.33), the above equation can simplified

$$I = \frac{S_{band}}{\omega_o} \qquad \ldots(4.40)$$

### 3.6 X-ray Diffraction (XRD) Analysis

X-ray diffraction (XRD) is a scientific tool and commonly used as it can provide information about phase identification, chemical composition and crystal size. It can also be used for quantitative analysis of phase compositions. The Siemens model D5000 X-ray Diffractometer is utilized in this work to obtain the spectrum of a-Si:H thin film deposited on both glass and crystal silicon substrates.

Normally the distance between two atoms is about 1 Å. If the ordered and periodic properties of a crystal occur only at a finite distance or the arrangement of the atoms in the material is defective, the crystalline structure is imperfect. Materials such as metals, stones, alloys and bones are crystals [20].

A polycrystalline material consists of a multitude of randomly oriented small crystals which are usually of different sizes and irregular shapes; they are called crystallites. It may be an aggregate of tightly bonded crystals, as in the case of metals, alloys and many minerals.

#### 3.6.1 XRD Measurement Technique

The source in XRD is an x-ray that is usually produced by a high-energy electron beam directed into a cooled metal target. The electrons have an inelastic

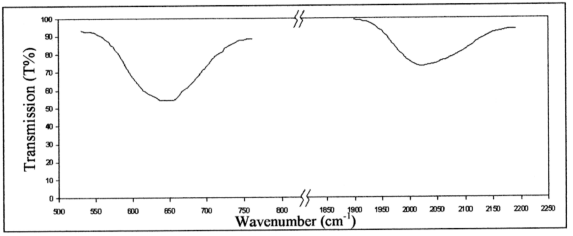


(a)

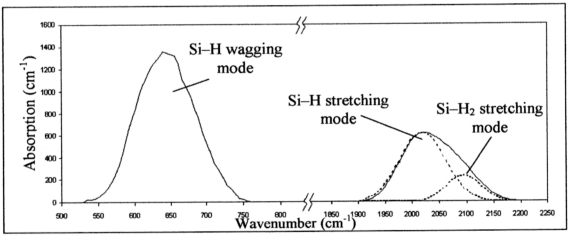


(b)

Figure 3.11: The FTIR spectroscopy showing the main peaks at 640 $cm^{-1}$ and 2000 $cm^{-1}$ of (a) transmission spectra (b) absorption spectra

collision within the metal target and the electrons decelerate and interact with the target atoms. The electron knocks out target electrons from their orbitals creating a high-energy excitation site. This state is brief and the electron soon falls to a lower energy state and emits an x-ray in the process. With several electrons bombarding the target x-ray of several different wavelengths are created. In this work, a monochromatic incident beam where only one wavelength of x-ray is used. Directing the x-ray through a foil filters out the other wavelengths. Different foils filter out different wavelengths so it is important to choose the correct foil for the wavelength desired. One can also monochromize the beam with a single crystal as a diffractor. The crystal can be set to diffract a certain wavelength by choosing different incident angles for the x-rays.

A diffracted beam is composed of many waves that have been scattered by atoms in a crystal that were in the path of the incident beam. Reflection is the bouncing back of visual light as a surface phenomenon in a layer that is about 1/2 thick. The diffraction of waves only occurs at certain angles, called Bragg angles, where Bragg's law is satisfied. In contrast, reflection takes place at any angle of incidence as illustrated in figure 3.12. The values of d and the number and types of atoms in each plane are unique for every mineral. With a diffracted beam the intensity is much smaller coming out of the crystal is significantly smaller than the initial intensity. Reflective beams have almost the same intensity coming out as going in.

Diffraction may or may not satisfy Bragg's Law. Diffraction satisfying Bragg's law occurs when the atoms are arranged periodically in space. The diffraction is in very few directions and is strong. The diffraction can also be in most directions, which does not satisfy Bragg's law. There is no scattering because the scattered rays cancel each other out because of distinctive interference. If atoms are arranged randomly, like in a monatomic gas, the scattering occurs in all directions and is weak. The direction of scattering is decided completely by the shape and size of the unit cell.

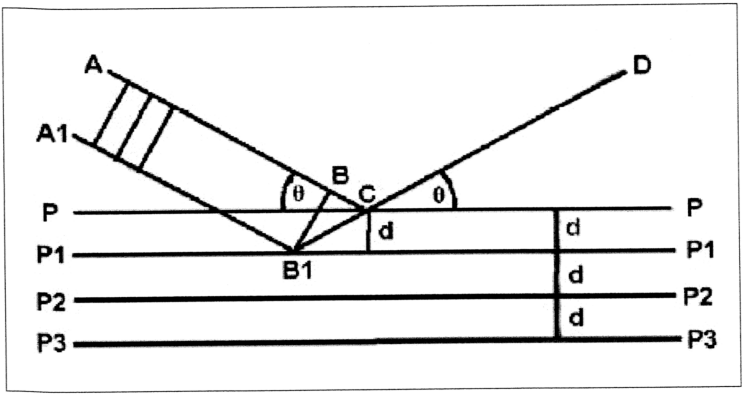


Figure 3.12: The principle of X-ray reflection

The intensity of the diffracted beam is decided by the position of the individual atoms within the unit cell.

### 3.6.2 Grain Size Calculation Technique

In this work, a new high-performance software, DIFFRAC plus is used to analyze the samples. The unique features of this software provides the information obtained from the measurement, such as peak widths, peak asymmetries, shoulders on the peaks and peaks with very low intensity. From these data, the average crystallite size of the sample can be calculated using Scherrer's equation,

$$D_x = \frac{\beta\lambda}{\Delta(2\theta)\cos\theta} \qquad \ldots(4.41)$$

where $\lambda$, $\Delta$ $(2\theta)$ and $\theta$ are the wavelength of the x-ray source ($Cu–K_\alpha$ = 1.542 Å), broadening at full width half maximum (FWHM) and angle diffraction peak respectively. $\beta$ is a constant and was taken as 0.9.

## 3.7 Atomic Force Microscopy (AFM) Analysis

Scanning force microscopy as the most widely used variant of the scanning probe methods exhibit a strikingly successful evolution over the past ten years. Today force microscopy and related methods are used in experimental physics, in chemistry, in materials science and in biology. While the basic modes of operation are well established and are available as commercial solutions, some highly dedicated modes of operation are permanently under development. In this work, the Digital Instruments Nanoscope model IIIa Atomic Force Microscopy (AFM) is used to study the morphology and the surface roughness of the a-Si:H thin film samples.

### 3.7.1 Atomic Force Microscopy (AFM) Technique

The key element of the AFM is the microscopic force sensor or cantilever as shown in figure 3.13, which is typically 200 μm long and 2 μm thick. Mounted on the end of the cantilever is a sharp tip, which is used to sense the force between the tip and the sample. The tip is brought into contact with the sample surface, which is scanned underneath the tip. The force experienced between the tip and sample causes a deflection of the cantilever, which in turn can be used to provide a topographical map of the surface.

Figure 3.14 shows the components of a scanning probe instruments. The whole system is controlled by a computer which creates the ramp signals for scanning and which serves for data acquisition, data analysis, data processing, and data visualization. The computer is linked to the microscope and to the peripheral electronics by DACs and ADCs. The peripheral electronics contains, apart from the feedback loop, suitable devices to measure the probe-sample interaction as well as the high-voltage amplifiers for driving the piezoelectric actuators.

In advanced systems the computer control also allows to employ numerous operational modes, which deviate from constant-interaction scanning. These modes involve scanning at a constant average probe-sample distance, local spectroscopy, the performance of local surface modifications by increasing the probe-sample interaction, and a variety of other features.

## 3.8 Dark-Conductivity Measurement

The dark-conductivity, σ of a-Si:H is often determined to evaluate the underlying electronic transport properties of thin-film samples. In this work, the experimental measurement of σ is performed using surface coplanar electrodes configuration as illustrated schematically in figure 3.15. Difficulties with this

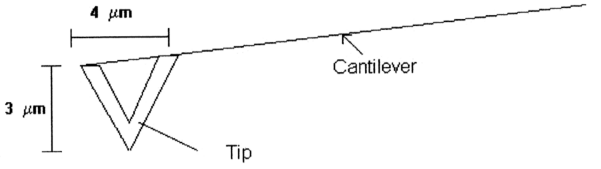


Figure 3.13: A Schematic of an AFM Tip and Cantilever

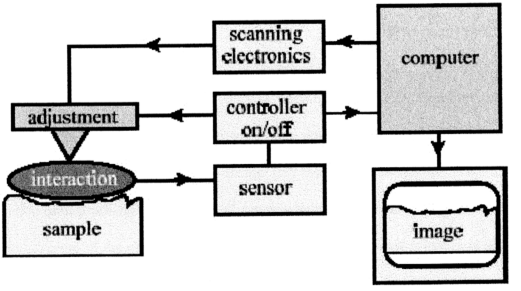


Figure 3.14: Components of a Scanning Probe Instruments

arrangement have been highlighted by Dawson et. al. [21] who emphasize that for particular contact geometries, carrier depletion in the a-Si:H film beneath the contact material may distort the conductivity parameters deduced from $\sigma(T)$ data. Provided sufficient care is taken to eliminate surface adsorption effects, the coplanar setup may still provide realistic estimates of true bulk conductance parameters. This has been demonstrated by Aker [22] who has evaluated the effect of chemisorption of ambient gas molecules on rf PECVD a-Si:H films.

### 3.8.1 Deposition of Aluminum Electrodes by Evaporation Process

The current-voltage (I-V) measurement done on the a-Si:H thin film is carried out at room temperature using aluminum electrodes in a co-planar configuration. These electrodes are prepared at Solid State Research Laboratory, University of Malaya by evaporation process. The schematic diagram of the electrodes on the a-Si:H thin film sample is shown in figure 3.15.

Figure 3.16 shows a schematic diagram of the system used to evaporate the electrodes. Initially, the roughing valve (V1), backing valve (V2), air admittance valve (AAV) and baffle valve (BF) are closed. Then small pieces of aluminum wires are placed on the spiral tungsten wire inside the evaporation chamber. The lines are evacuated until a pressure of $1.0 \times 10^{-3}$ mbar is achieved. V1 and V2 are then opened and the pressure of the chamber is monitored. When the chamber pressure is about $1.0 \times 10^{-3}$ mbar, the diffusion pump is ready to be activated. Before switching on the diffusion pump, it is necessary to turn on the water supply for the water-cooling system. A fan is also turned on to enhance the cooling process. After about 20 minutes, V1 is closed and BF is opened. The system is now ready for the evaporation process of the aluminum when the chamber pressure has reached $10^{-5}$ mbar.

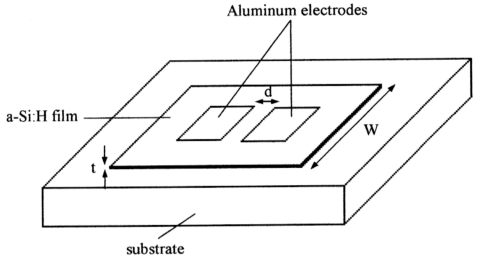


(a)

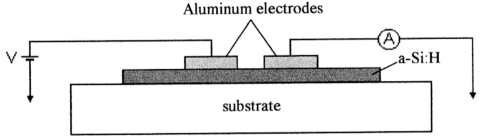


(b)

Legend:

d = distance between electrodes
W = width of the electrodes
t = thickness of the a-Si:H sample

Figure 3.15: The co-planar configuration of the aluminium electrodes on the a-Si:H film. (a) 3-D view (b) side view

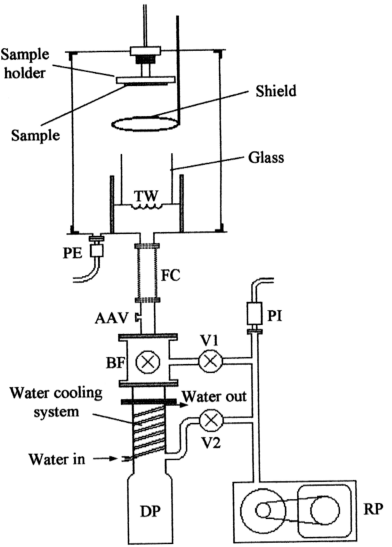


Legend:

AAV = Air admittance valve
BF = Baffle valve
DP = Edwards diffusion pump
FC = Edwards flexible couplings
PE = Edwards Penning CP25K gauge head
PI = Edwards Pirani PRM 10 gauge head
RP = Edwards EM 5 rotary pump
TW = Tungsten wire
V1 = Edwards Speedivalve (roughing valve)
V2 = Edwards Speedivalve (backing valve)

Figure 3.16: The evaporation system to deposit alluminium electrodes

A high voltage is applied across the tungsten wire passing a high current through it. The wire glows heating up the aluminum wires and as soon as the melting temperature is reached, the aluminum wires evaporate. Initial evaporation is blocked from the samples to eliminate impurities. The shield is removed after a few seconds to allow pure aluminum to be evaporated as electrodes on to the samples.

### 3.8.2 Current-Voltage (I-V) Measurement Technique

In this work, Keithley 236 Source Measure Unit (SMU) is used to measure the current-voltage (I-V) of the samples. This experimental is done at room temperature in the dark condition. The SMU is connected to the computer via IEEE-488 interface card. The experimental set-up is shown schematically in figure 3.17. To operate the SMU, the computer should have Windows 3.0 or 3.1 and a Metric Software. Metrics is a uniquely powerful instrumentation control and data analysis software package. Metrics is designed to control semiconductor test equipment used for device characterization and other microelectronic testing.

The sample is placed on the Signatone H150 Probe Station which also equipped with Olympus SZ-STU2 Microscope to view the contact between the probe and the sample. The circuit is as illustrated in figure 3.15b. Before starting any measurement, it is necessary to empty traps in the sample. For this sample, this can be done by applying a voltage of about 70 V to the sample for at least eight hours. The voltage is initially set and the current which flow through the sample is measured automatically by the SMU.

### 3.8.3 Dark-conductivity Calculation Technique

The current-voltage (I-V) curve obtained from above technique is plotted in ohmic region. The ohmic region can be distinguished from plot of log I versus log V where its slope is equal to 1. Subsequently, the conductivity of the sample in that

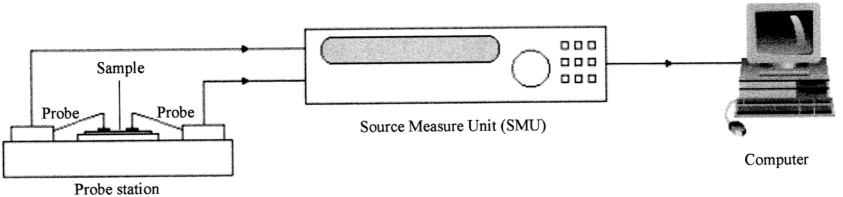


Figure 3.17: An experimental set-up for I-V measurement

particular region can be calculated

$$\sigma = \frac{I}{V}\frac{L}{A} \text{ Scm}^{-1} \qquad \ldots(4.42)$$

where L is the width of the gap between the electrodes and A is the cross section area perpendicular to the direction of the current flow.

## 3.9 References


1. P. Roca i Cabarrocas, "Growth of undoped a-Si:H by PECVD" EMIS Datareviews Series No. **19**, (1997) 3-10.
2. Namaoui Mohamed, MSc. Thesis, University of Malaya, (1999).
3. Aniszawati Azis, MSc. Thesis, University of Malaya, (2000)
4. Wong King Seng, MSc. Thesis, University of Malaya, (1992).
5. UV-Visible Spectrometers Instruction Manual.
6. J.C. Manifacier, J. Gasiot and J.P. Fillard, J. Phys. E, **9**, (1976) 1002.
7. R. Swanepoel, J. Phys. E, **16**, (1983) 1214-1222.
8. E.A. Davis, N. Piggins, S.C. Bayliss, J. Phys. C, **20**, (1987) 4415-4427.
9. Wemple, DiDomenico, Phys. Rev. B, **3**, (1971) 1338.
10. C. Ance, J.P. Ferraton, J.M. Berger and F. de Chelle, Phys. Stat. Sol. (b), **113**, (1982) 105.
11. S.A. Rahman, PhD. Thesis, University of Malaya, (1995).
12. M. H. Brodsky, R.S. Title, K. Weiser and G.D. Pettit, Phys. Rev. B, **1**, vol. **6** (1970) 2632-2641.
13. J. Tauc, R. Grigorovici and A. Vancu, Phys. Stat. Sol., vol. **15** (1966) 627-637.
14. S. Hasegawa, H. Anbutu and Y. Kurata, J. Non-Cryst. Sol. vol. **97** (1987) 1043-1046.

15. F. Urbach, Phys. Rev., **92** (1953) 1324.

16. J. Tauc, "Infrared and Raman Spectroscopy of Amorphous Semiconductors" in "Physics of Structurally disordered Solids" ed. S.S. Mitra, Plenum Press (1976) 526.

17. Shanks H., C.J. Fang, Ley L., M. Cardona, F.J. Demond and S. Kalbitzer, Phys. Stat. Sol. (b), **100** (1980) 43.

18. P. Gans, Data Fitting in the Chemical Sciences, John Wiley and Sons (1992).

19. P.W. Milonni and J.H. Eberly, Lasers, John Wiley and Sons (1991).

20. Md. Rahim Sahar, "Pengenalan Kaji Logam Sinar-X", Dewan Bahasa dan Pustaka, 1993.

21. R. Dawson, S. Nag, M Gunes, C. Wronski, Mater. Res. Soc. Symp. Proc. (USA) vol. **258**, (1992) 747.

22. B. Aker, Philos. Mag. B (UK) vol. **55**, (1987) 313.